High-pressure torsion of hafnium

Edalati, Kaveh
Department of Materials Science and Engineering, Faculty of Engineering, Kyushu University

Horita, Zenji
Department of Materials Science and Engineering, Faculty of Engineering, Kyushu University

Mine, Yoji
Department of Mechanical Engineering, Faculty of Engineering, Kyushu University | Research Center for Hydrogen Industrial Use and Storage (HYDROGENIUS), National Institute of Advanced Industrial Science and Technology (AIST)

出版情報：Materials Science and Engineering : A. 527 (7/8), pp.2136-2141, 2010-03-25. Elsevier
バージョン：

High-pressure torsion of hafnium

Kaveh Edalati[a,*], Zenji Horita[a], Yoji Mine[b,c]

[a] Department of Materials Science and Engineering, Faculty of Engineering, Kyushu University, Fukuoka 819-0395, Japan

[b] Department of Mechanical Engineering, Faculty of Engineering, Kyushu University, Fukuoka 819-0395, Japan

[c] Research Center for Hydrogen Industrial Use and Storage (HYDROGENIUS), National Institute of Advanced Industrial Science and Technology (AIST), Fukuoka 819-0395, Japan

Abstract

Pure Hf (99.99%) is processed by high-pressure torsion (HPT) under pressures of 4 and 30 GPa to form an ultrafine-grained structure with a gain size of ~180 nm. X-ray diffraction analysis shows that, unlike Ti and Zr, no ω phase formation is detected after HPT processing even under a pressure of 30 GPa. A hydride formation is detected after straining at the pressure of 4 GPa. The hydride phase decomposes either by application of a higher pressure as 30 GPa or by unloading for prolong time after HPT processing. Microhardness, tensile and bending tests show that a high hardness (360 Hv) and an appreciable ductility (8%) as well as high tensile and bending strength (1.15 and 2.75 GPa, respectively) are achieved following the high-pressure torsion.

Keywords: Hafnium; Hydrides; Hydrogen; High-pressure torsion; Severe plastic deformation; Ultrafine-grained structure

*Corresponding author. Tel.: +81 092 802 2992; fax: +81 092 802 2992.

E-mail address: kaveh.edalati@zaiko6.zaiko.kyushu-u.ac.jp (K. Edalati).

1. Introduction

Severe plastic deformation (SPD) is a useful procedure for significant refinement of microstructures in metallic materials [1]. To achieve ultrafine-grained (UFG) metals with high strength and reasonable ductility, a great attention has been allocated to the application of high-pressure torsion (HPT) [2–8]. Despite numerous researches of the HPT processing for different pure metals, there is no report for pure Hf. It is well known that Hf is a heavy metal with a density of 13.3 g cm^{-3} and can be promising as Ti and Zr for biomedical materials and surgical implants because of high corrosion resistance good biocompatibility and osteoconductivity provided that the strength to weight ratio is improved [9]. It is also known that Hf exhibits, as Ti and Zr, a phase transformation from an ω phase with the hcp crystal structure to an ω phase with the simple hexagonal structure at a high pressure [10–16]. Whereas the critical pressure for the formation of the ω phase is in the range of 2–11 GPa in Ti and Zr [11–16], it is higher as ~21 GPa [11] or 38±8 GPa for Hf [12,13]. Furthermore, the ω phase is retained as a metastable phase at ambient pressure after unloading in Ti and Zr but this is not in Hf because of the ω→α reverse transformation upon unloading. Earlier studies reported that shear strain under an application of high pressure facilitates the α→ω phase trans- formation in Ti and Zr and thus increases the fraction of ω phase [7,17–21]. It may be then anticipated that an α→ω phase transformation is induced in Hf by straining under a high pressure and the ω phase may be present at ambient pressure as a metastable phase.

It is also well known that Hf absorbs hydrogen as Ti and Zr and forms a hydride phase with a crystal structure based on fcc and fct [22–24]. It was reported that the formation of the hydride phase in Zr was induced by straining, resulting in a ductility loss even when the hydrogen content is fairly low [25]. To the best of the authors' knowledge, little is understood regarding the strain-induced phase transformation in Hf including the influence of pressure on the hydride formation. In this study, thus for the first time, pure Hf is severely deformed by HPT over a wide range of strain under high pressures. Evolutions of microstructures and mechanical properties are investigated with a special attention on phase transformation and hydride formation as a consequence of HPT operation.

2. Experimental materials and procedures

Square-shaped chips of pure Hf (99.99%) with dimensions of 10mm×10mm×1.05mm having impurity of 0.08 wt.% Fe were purchased for this study. The chips were first annealed for 1 h at 1000 °C in an argon atmosphere for eliminating deformation history involved in the chips. The square chips were enclosed in an evacuated silica glass tube and were further annealed at 400 °C for 5 h in order to remove any possible formation of hydride during handling as it was reported that the hydride is decomposed rapidly by the annealing at the temperatures above 327 °C [22,23]. Samples after annealing were cut to discs with diameters of 3 and 10 mm using a wire-cutting electric discharge machine.

HPT was conducted at room temperature on the annealed discs. Two sets of upper and lower anvils with a circular flat-bottom hole at the center having a nitrified surface with the roughness of ~30 μm were used to process the disc samples. The hole depths were 0.15 and 0.35mmand the hole

diameters were 3 and 10mm, respectively. The disc samples with 10mm diameters were processed for N = 0, 1, 3 and 10 revolutions under a pressure of 4 GPa and the disc samples with 3mmdiameters were processed for N = 0, 1 and 3 revolutions at 30 GPa. The rotation speed was 0.2 rpm for both 3 and 10mm diameter discs.

The HPT-processed discs with 10mm diameter were evaluated using Vickers microhardness measurement, tensile test, bending test, transmission electron microscopy (TEM), X-ray diffraction (XRD) analysis and thermal desorption spectrometry (TDS) analysis and those with 3mm diameter by XRD. First of all, after processing by HPT, the 10mm discs were polished to a mirror-like surface and the Vickers microhardness was measured with an applied load of 200 g for 15 s along the radii from the center to edge at 8 different radial directions with 0.5mm increments as drawn by dotted lines in Fig. 1. Second, miniature tensile specimens having 1.5mm gauge length, 0.7mm width and 0.5mm thickness were cut from the 10mm discs at the position 2mm away from the center as illustrated in Fig. 1. Each tensile specimen was mounted horizontally on grips and pulled to failure using a tensile testing machine with an initial strain rate of 2×10^{-3} s^{-1}. It should be noted that the dimensions of the present tensile specimens are fairly small and therefore, care is required when compared with other dimensions of tensile specimens as pointed out by Zhao et al. [26]. Third, for bending tests, miniature rods with a 0.5mmsquare cross section and 9mmlength were cut from the 10mm diameter discs at 1mm away from the disc center as illustrated in Fig. 1. Three-point bending tests were carried out at room temperature to measure the bending load and displacement of samples in both radial direction and pressing direction for individual HPT conditions. The supporting span was 8mm and the stroke was controlled at a cross-head speed of 0.5 mm/s.

The bending stress was calculated from the load and the specimen geometry through the following equation [27]:

$$\sigma = \frac{3Pl}{2bh^2} \qquad (1)$$

where P is the bending load, l is the supporting span (8 mm), b is the bending specimen width (0.5mm) and h is the bending specimen height (0.5 mm). Fourth, for XRD and TDS, 3mm discs were prepared from as-received and annealed materials as well as from 3 and 10mm HPT-processed discs. Discs with 3mm diameter were punched out from the 10mm discs at 3.5mm away from the center as shown in Fig. 1. The 3mm discs were ground and polished mechanically to a thickness of 0.5 mm very smoothly and XRD was performed on these samples using the Co Kα radiation at 40 kV and 36 mA in a scanning step of 0.02° and a scanning speed of 0.4 °/min. TDS was carried out for the hydrogen measurement as a function of the sample temperature from 56 to 850 °C at a heating rate of 0.17 °C/s. For TEM, the 3mm diameter discs used for the XRD were ground mechanically to a thickness of 0.15 mm and further thinned with a twin-jet electro-chemical polisher using a solution of 10% $HClO_4$ and 90% CH_3COOH at 25 °C. TEM was performed at 200 kV for microstructural observation and for recording selected-area electron diffraction (SAED) patterns.

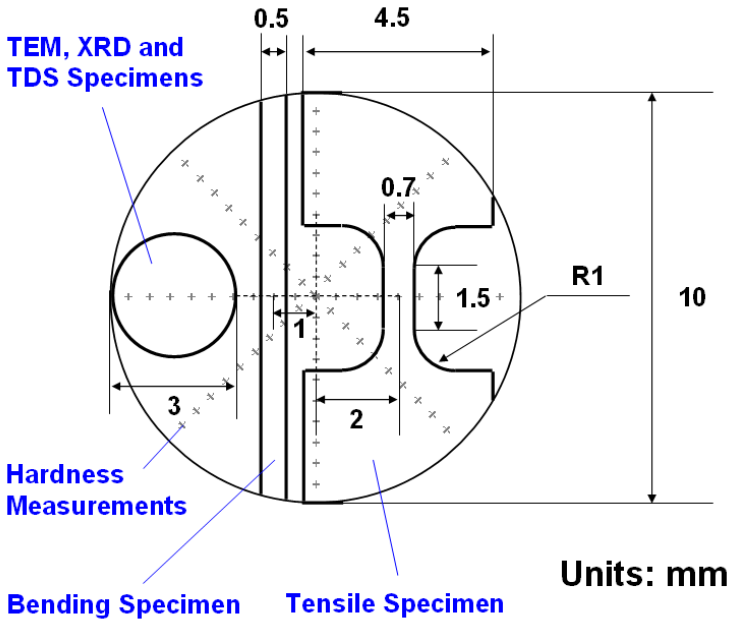

Fig. 1. Schematic illustration of HPT discs and procedures for microhardness measurements, and dimensions and locations for tensile and bending testing specimens and for TEM, XRD and TDS disc.

3. Results and discussions

The variations of hardness are plotted in Fig. 2 against the distance from the disc center for N = 1, 4, 10 and 40 revolutions under a pressure of (a) 2 and (b) 6 GPa. Microhardness increases with the distance from the disc center for all numbers of revolutions and for both pressures. Microhardness increases with the numbers of revolutions after processing with HPT at 2 GPa; whereas, hardness increases with an increase in the numbers of revolutions from 1 to 4 after processing at 6 GPa but the hardness level decreases for larger numbers of revolutions from 4 to 10 through 40. All microhardness values in Fig. 2 are plotted against the equivalent strain in Fig. 3. Here, the equivalent strain was calculated by the equation as [28]:

$$\varepsilon = (1-s)\int_0^N \frac{2\pi r}{\sqrt{3}\, t(N)}\, dN \qquad (2)$$

where r is the distance from the center of disc, N is the number of revolutions, s is the fraction of sample slippage, as described earlier [29], and $t(N)$ is the thickness of disc as a function of N determined by fitting of experimentally measured thicknesses. It is apparent from Fig. 3 that all microhardness data points tend to fall on a single curve. The hardness increases with increasing equivalent strain at an early stage of straining but saturates to a steady state at high strains where the hardness remains unchanged with further straining. The microhardness at the steady state is 360 Hv. The shape of the hardness versus strain curve for pure Hf is similar to those for Cu [30], Fe [28], Ti [20] and Zr [21]. It was considered that the saturation stage (steady state) appears because of a balance between the hardening and the softening, where the hardening is due to dislocation accumulation and grain refinement whereas the softening due to annihilation of dislocations through recovery [31,32] or recrystallization [2,33].

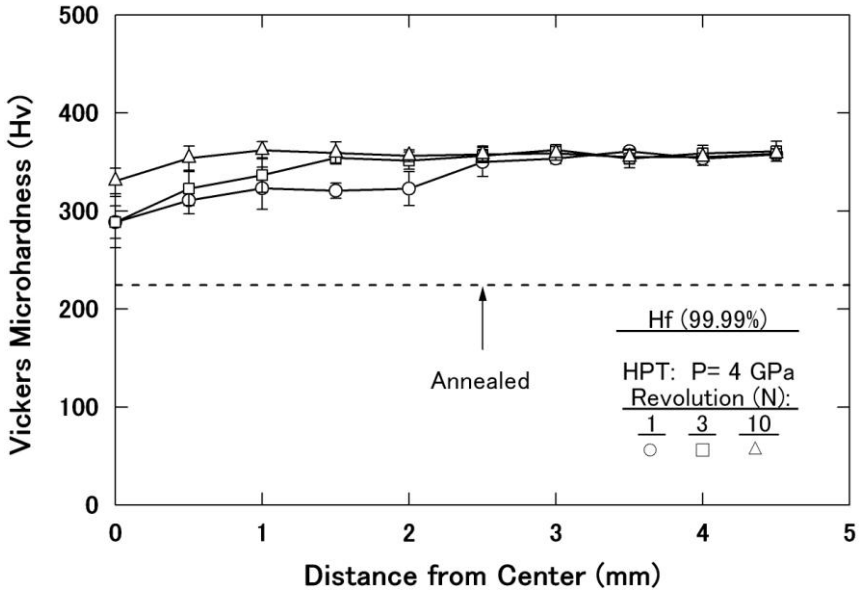

Fig. 2. Vickers microhardness plotted against distance from center for samples processed under a pressure of 4 GPa and various revolutions.

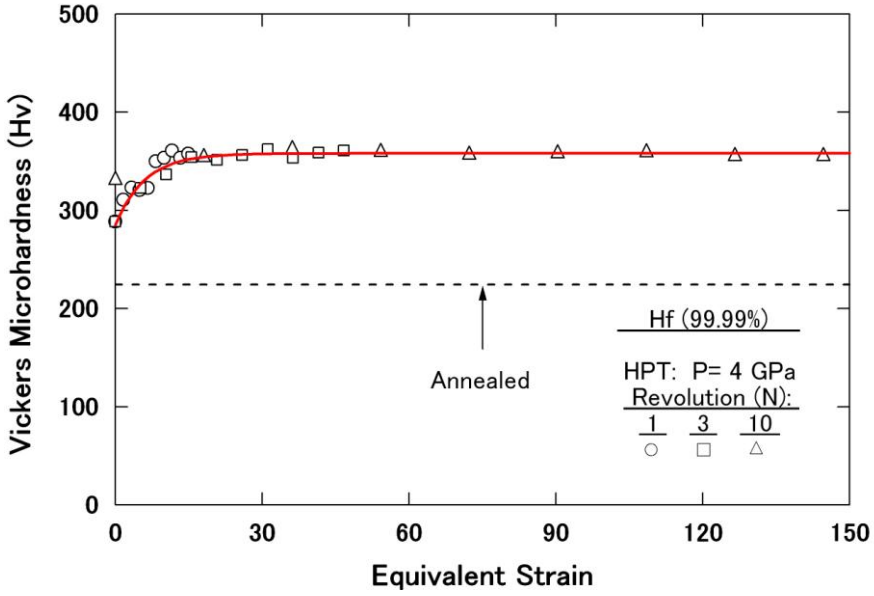

Fig. 3. Vickers microhardness plotted against equivalent strain for samples processed under a pressure of 4 GPa and various revolutions.

The stress–strain curves for annealed sample as well as HPT samples processed for N = 1, 3 and 10 revolutions under a pressure of 4 GPa are delineated in Fig. 4 from tensile tests conducted at room temperature at an initial strain rate of 2×10^{-3} s^{-1}. The tensile strength increases and the total elongation to failure remains almost unchanged with an increase in the number of revolutions or an increase in the equivalent strain. The annealed sample exhibits the tensile strength similar to the one in an earlier report after annealing [24]. For HPT-processed samples, the tensile strength is expressed by the hardness through the relation as $\sigma = 3.2Hv$ where the factor, 3.2, is consistent with

the factor, ~3, accepted for the conversion for many materials. It is also found that the strength to weight ratio for Hf after processing with HPT for N = 10 revolutions is 86 J/g which is 3.5 times as high as the annealed one. This strength to weight ratio of pure Hf is well comparable with that of commercially pure Ti which is 52 J/g for Grade 1 and 148 J/g for Grade 4B corresponding to ISO 5832-2 standard for implant materials [34].

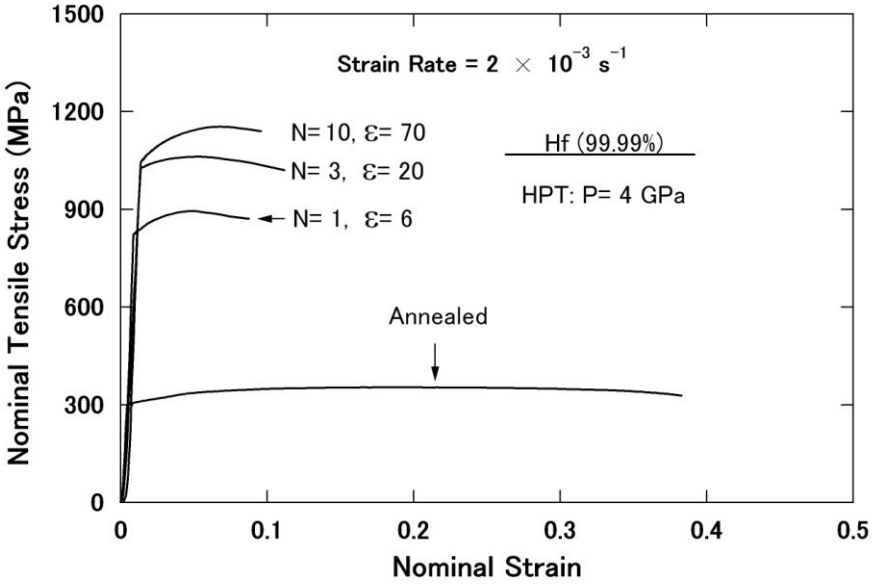

Fig. 4. Nominal tensile stress versus nominal strain curves for annealed sample and samples processed under a pressure of 4 GPa and various revolutions.

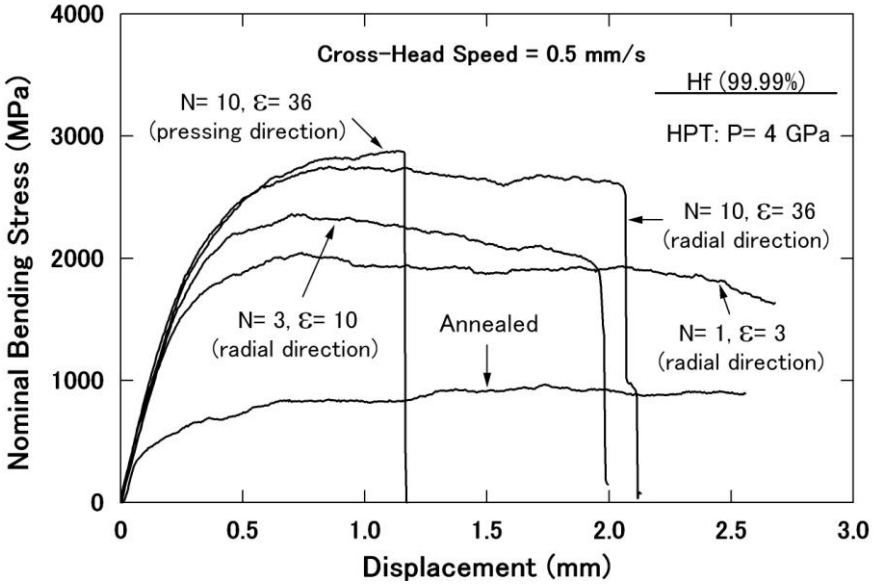

Fig. 5. Nominal bending stress versus displacement curves for annealed sample and samples processed under a pressure of 4 GPa and various revolutions.

Fig. 5 delineates the stress-displacement curves obtained from bending tests at room temperature with a cross-head speed of 0.5mm/s for samples processed for N = 1, 3 and 10 revolutions under a

pressure of 4 GPa including an annealed sample before HPT. Examination of Fig. 5 indicates three important points: (1) the bending strength significantly increases by processing with HPT while the ductility remains reasonably large when compared with the annealed sample; (2) the bending strength increases with an increase in the equivalent strain but the total displacement to failure decreases as the equivalent strain increases from 3 to 10 and slightly decreases with a further increase in the equivalent strain from 10 to 36; and (3) the bending strengths for both radial direction and pressing direction are the same but the total displacement to failure in the radial direction is higher than that in the pressing direction. Comparison of Fig. 5 with Figs. 3 and 4 shows that the bending strength has the same trend as the hardness and the tensile strength with respect to strain.

TEM microstructures are shown in Fig. 6 for the sample after HPT processing for N = 10 revolutions under the pressure of 4 GPa. A bright-field image and a dark-field image including the corresponding SAED pattern are shown for this sample in (a), (b) and (c), respectively. Note that the dark-field image was taken with the diffracted beam indicated by an arrow in the SAED pattern. It should be noted that the microstructure in Fig. 6 corresponds to the steady state in the plot of hardness against equivalent strain shown in Fig. 3. It is apparent from Fig. 6 that the microstructure consists of small grains having high angles of misorientation as evident from the SAED with a well-defined ring pattern. Close examination of the microstructures reveals that there are many dislocations within the grains and most of the grains are surrounded by curved and ill-defined grain boundaries.

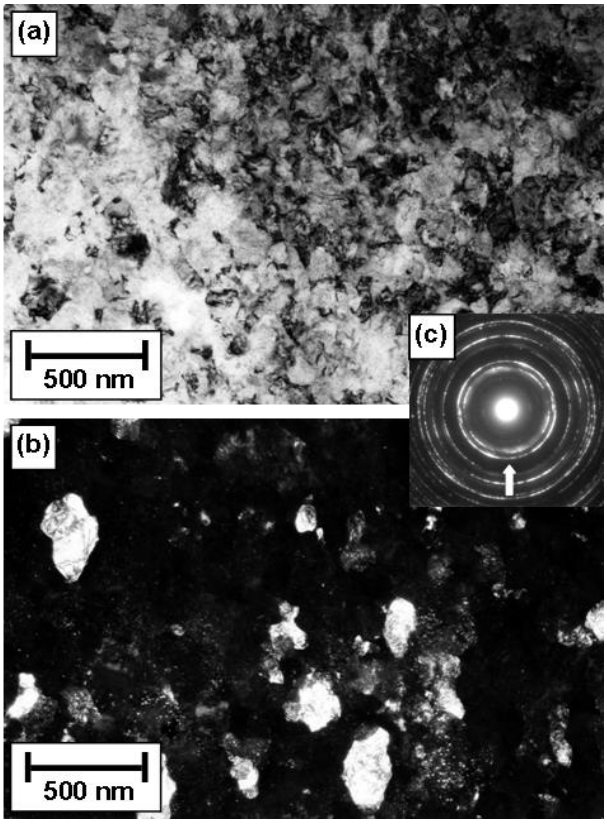

Fig. 6. TEM (a) bright- and (b) dark-field images and SAED pattern for sample processed under a pressure of 4 GPa after 10 revolutions.

The grain size distribution after 10 revolutions under a pressure of 4 GPa is shown in Fig. 7, which was obtained from the dark-field image similar to Fig. 6(b) by measuring the two orthogonal axes of the bright areas corresponding to a total of 260 grains. It is found that the sizes of all measured grains are in the nanometer or sub-micrometer range and the average grain size is ~180 nm. These microstructural features of Hf are similar to the earlier observation of Ti and Zr [20,21].

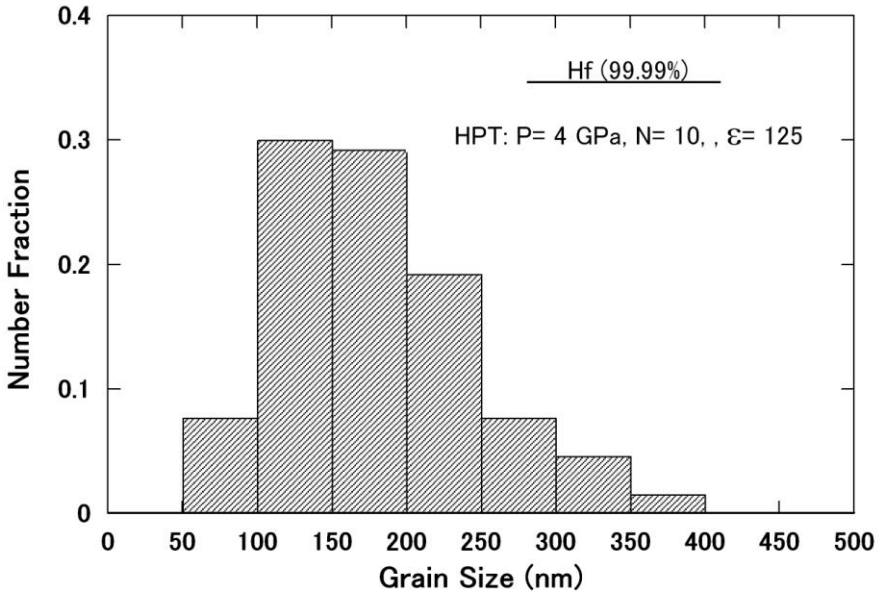

Fig. 7. Number fraction of grain size distribution for sample processed under a pressure of 4 GPa after 10 revolutions.

XRD profiles are shown in Fig. 8 for the samples after annealing at 1000 °C for 1 h, and after HPT processing at 4 GPa for N = 10 revolutions and at 30 GPa for N = 0 and 1 revolutions. Three points should be noted for Fig. 8: (1) no peak associated with the ω phase is visible at any conditions including after application of 30 GPa: (2) peaks of hafnium hydride (HfH_2) are present after annealing at 1000 °C and after processing at 4 GPa; and (3) such hydride peaks disappear by HPT processing after application of 30 GPa.

Regarding the first point, the absence of the ω phase suggests that no transformation occurs from α phase to ω phase through HPT processing, or the phase transformation occurs but the reverse transformation from ω phase to α phase follows upon unloading or quickly after unloading. Based on the dynamical observations reported earlier using a diamond anvil cell at a pressure more than 21 GPa [11,12] or 38±8 GPa [13], it is considered that the latter should be the case and it is suggested that, unlike Ti and Zr reported earlier [7,17–21], straining under high pressure is not effective in Hf to facilitate the phase transformation or to stabilize the _ phase after unloading.

The second and third points indicate that the hydride phase is decomposed by application of a high pressure at 30 GPa. The decomposition of the hydride phase was reported in the Cu–H system at high pressures due to thermodynamic instability [35,36]. It is considered that the hydride phase may decompose either during application of the high pressures or after unloading.

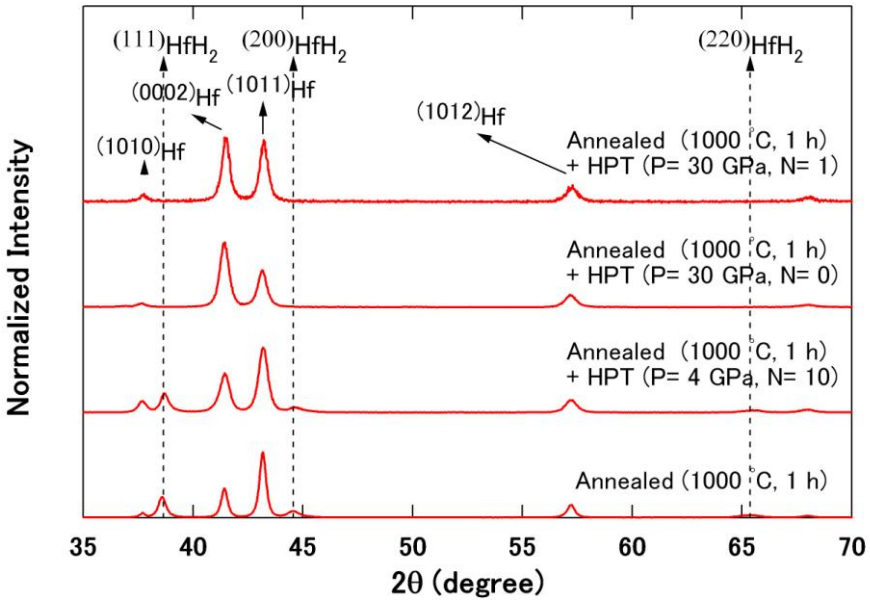

Fig. 8. XRD profiles of Hf after annealing at 1000 °C for 1 h, after HPT processing at 4 GPa for N = 10 revolutions and after HPT processing at 30 GPa for N = 0 and 1 revolutions.

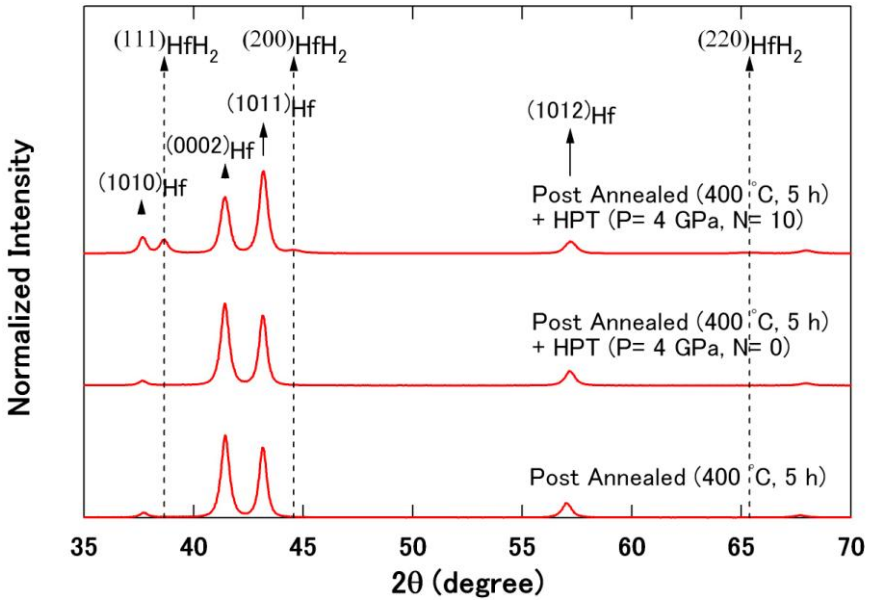

Fig. 9. XRD profiles of Hf after post-annealing at 400 °C for 5 h and after HPT processing at 4 GPa for N = 0 and 10 revolutions.

According to the reports that the hydride phase is also decomposed at temperatures above 327 °C [22,23], some samples were annealed at 400 °C for 5 h. As shown in Fig. 9, the hydride phase disappears by this post-annealing. The samples after the post-annealing were then processed by HPT at 4 GPa for N = 0 revolutions and for N = 10 revolutions. No hydride peak appears after application of 4 GPa without straining (N = 0), but the hydride peak is detected after HPT processing for N = 10 revolutions. Thus, the results indicate that strain-induced hydride formation

has occurred as reported in Zr [25], Ti [37,38], Nb [39,40] and V [41]. Hydrogen atoms diffuse through the lattice since the atomic diameter is much smaller than any of the other metallic atoms. However, transported hydrogen can accumulate in microstructural defects such as voids, dislocations and grain boundaries which are known as trapping sites for hydrogen [42]. Thus, the hydrogen concentration may locally exceed a limit for the hydride formation in the strain field, leading to the hydride formation even when the average hydrogen content is fairly low [40,43–45].

The hydride formation is also confirmed by the two TDS spectra as shown in Fig. 10, where the samples subjected to post-annealing were analyzed by TDS before and after HPT processing at 4 GPa for 10 revolutions. It is apparent that the TDS peak in the spectrum shifts to a lower temperature by processing with HPT. This shift is due to desorption of hydrogen through the quick decomposition of the hydride at a temperature around 327 °C. It should be noted that the samples were mechanically polished and cleaned before TDS analysis to avoid any possible effect due to surface corrosion products [46].

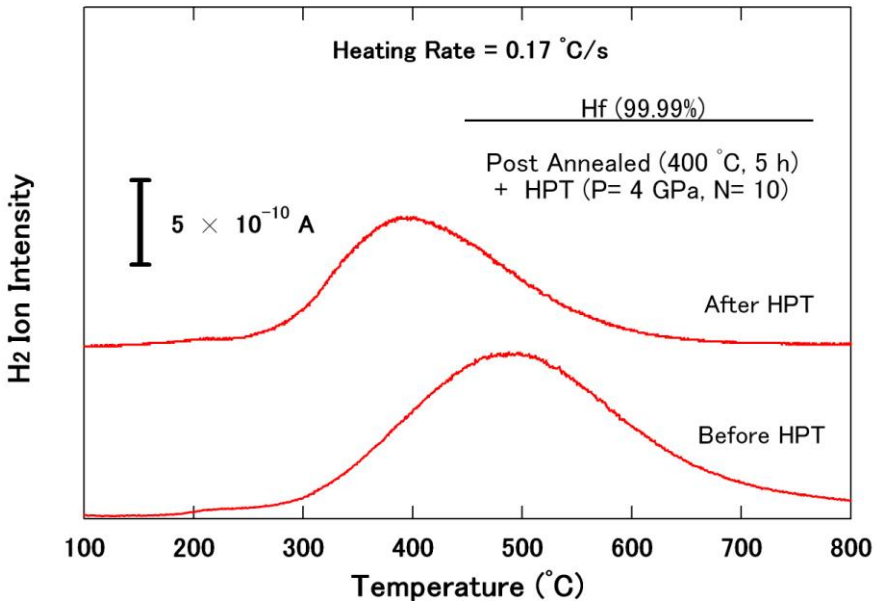

Fig. 10. TDS spectra of Hydrogen for samples post-annealed at 400 °C for 5 h and processed with HPT at 4 GPa for N = 10 revolutions obtained before and after HPT.

Experiments were further carried out with the samples of hydride formation after processing by HPT at 4 GPa for 10 revolutions. Such samples were then kept for 2 h and 10 days following the HPT processing and XRD profiles of the corresponding samples are shown in Fig. 11. Comparison reveals that the hydride peaks clearly disappear after storage for 10 days. This indicates that strain-induced hydride phase is metastable and decomposes during storage in the ambient pressure after HPT processing.

In summarizing the hydride formation, high pressure promotes the decomposition of hydride phase, whereas the strain promotes the formation of a metastable phase even when the average hydrogen content is fairly less than solvus level. The pressure and strain affect an opposite way for

the formation of the hydride phase in HPT operation so that the hydride formation may be controlled by the balance between the two factors. In this study, it was not possible to introduce large strain under the application of 30 GPa to detect a hydride phase because of a limited capacity for HPT operation, the presence of the hydride formation was clearly confirmed after 10 revolutions under the pressure of 4 GPa.

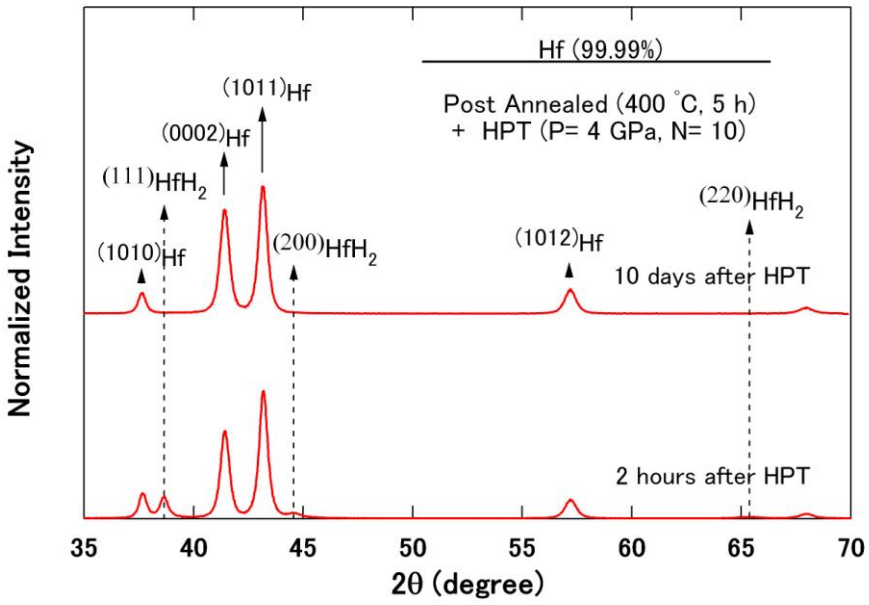

Fig. 11. XRD profiles of Hf post-annealed at 400 °C for 5 h and processed with HPT at 4 GPa for *N* = 10 revolutions obtained 2 h after HPT and 10 days after HPT.

4. Conclusions

High-pressure torsion (HPT) was conducted on pure Hf (99.99%) at applied pressures of 4 and 30 GPa and the following conclusions were obtained.

1. Vickers microhardness measurements revealed that the hardness increases with an increase in the equivalent strain at an early stage of straining and saturates into a steady state level at high strains.
2. Tensile and bending tests showed that an appreciable ductility as well as high tensile and bending strength (1.15 and 2.75 GPa, respectively) is achieved for the samples processed at 4 GPa.
3. TEMobservation showed that the average grain size at the steady state for the pressures of 4 GPa is ~180 nm.
4. XRD analysis revealed that no α→ω phase transformation is detected after processing at 4 and 30 GPa. This indicated that, unlike Ti and Zr, straining under high pressure is not effective in Hf to facilitate the phase transformation or to stabilize the ω phase after unloading.
5. XRD analysis also revealed that a strain-induced hydride phase forms by processing with HPT at 4 GPa. However, because the hydride phase is metastable it is decomposed by either storage after releasing the pressure or by application of a higher pressure as 30 GPa.

Acknowledgements

We would like to thank Prof. Kenji Higashida of Kyushu University for permitting the use of the bending test facility and Dr. Masaki Tanaka of Kyushu University for helpful assistance in using a bending test machine. One of the authors (KE) would like to thank the Islamic Development Bank for a scholarship. This work was supported in part by a Grant-in-Aid for Scientific Research from the Ministry of Education, Culture, Sports, Science and Technology, Japan in Priority Areas "Giant Straining Process for Advanced Materials Containing Ultra-High Density Lattice Defects", in part by the NEDO Fundamental Research Project on Advanced Hydrogen Science (2006–2012) and in part by Kyushu University Interdisciplinary Programs in Education and Projects in Research Development (P&P).

References

[1] R.Z. Valiev, R.K. Islamgaliev, I.V. Alexandrov, Prog. Mater. Sci. 45 (2000) 103–189.

[2] T. Hebesberger, H.P. Stuwe, A. Vorhauer, F. Wetscher, R. Pippan, Acta Mater. 53 (2005) 393–402.

[3] A.P. Zhilyaev, S. Lee, G.V. Nurislamova, R.Z. Valiev, T.G. Langdon, Scr. Mater. 44 (2001) 2753–2758.

[4] R.Z. Valiev, Y.V. Ivanisenko, E.F. Rauch, B. Baudelet, Acta Mater. 44 (1996) 4705–4712.

[5] A.P. Zhilyaev, T.R. McNelley, T.G. Langdon, J. Mater. Sci. 42 (2007) 1517–1528.

[6] A.V. Sergueeva, V.V. Stolyarov, R.V. Valiev, A.K. Mukhrjee, Scr. Mater. 45 (2001) 747–752.

[7] M.T. Perez-Prado, A.A. Gimazov, O.A. Ruano, M.E. Kassnerc, A.P. Zhilyaev, Scr. Mater. 58 (2008) 219–222.

[8] Y. Harai, Y. Ito, Z. Horita, Scr. Mater. 58 (2008) 469–472.

[9] M. Hironobu, Y. Atsuro, W. Fumio, U. Motohiro, K. Takao, Biomaterials 22 (2001) 1253–1262.

[10] Y.K. Vohra, J. Nucl. Mater. 75 (1978) 288–293.

[11] A.R. Kutsar, Fiz. Metal. Metalloved. 40 (1975) 786–793.

[12] S.K. Sikka, Y.K. Vohra, R. Chidambaram, Prog. Mater. Sci. 27 (1982) 245–310.

[13] H. Xia, G. Parthasarathy, H. Luo, Y.K. Vohra, L. Ruoff, Phys. Rev. B 42 (1990) 6736–6738.

[14] Y.K. Vohra, S.K. Sikka, S.N. Vaidya, R. Chidamberan, J. Phys. Chem. Solids 38 (1977) 1293–1296.

[15] C.W. Greeff, D.R. Trinkle, R.C. Albert, J. Appl. Phys. 60 (2001) 2221–2226.

[16] D. Errandonea, Y. Meng, M. Somayazulu, D. Haussermann, Physica B 355 (2005) 116–125.

[17] V.A. Zilbershtein, N.P. Chistotina, A.A. Zharov, N.S. Grishina, E.I. Estrin, Fiz. Metal. Metalloved. 39 (1975) 445–447.

[18] A.R. Kilmametov, A.V. Khristoforova, G. Wilde, R.Z. Valiev, Z. Kristallogr. Suppl. 26 (2007) 339–344.

[19] Y. Todaka, J. Sasaki, T. Moto, M. Umemoto, Scr. Mater. 59 (2008) 615–618.

[20] K. Edalati, E. Matsubara, Z. Horita, Metall. Mater. Trans. A 40 (2009) 2079–2086.
[21] K. Edalati, Z. Horita, S. Yagi, E. Matsubara, Mater. Sci. Eng. A 523 (2009) 277–281.
[22] B. Tsuchiya, M. Teshigawara, K. Konashi, S. Nagata, T. Shikama, J. Alloys Compd. 446/447 (2007) 439–442.
[23] B. Tsuchiya, Y. Arita, H. Muta, K. Kurosaki, K. Konashi, S. Nagata, T. Shikama, J. Nucl. Mater. 392 (2009) 464–470.
[24] J.R. Davis, Metals Handbook, ASM International, Materials Park, OH, 1998.
[25] C.D. Cann, E.E. Sexton, Acta Metall. 28 (1980) 1215–1221.
[26] Y.H. Zhao, Y.Z. Guo, Q. Wei, A.M. Dangelewicz, C. Xu, Y.T. Zhu, T.G. Langdon, Y.Z. Zhou, E.J. Lavernia, Scr. Mater. 59 (2008) 627–630.
[27] ASTM E290, Standard Test Methods for Bend Testing of Material for Ductility, ASTM International, West Conshohocken, PA, 2009.
[28] K. Edalati, T. Fujioka, Z. Horita, Mater. Trans. 50 (2008) 44–50.
[29] K. Edalati, Z. Horita, T.G. Langdon, Scr. Mater. 60 (2009) 9–12.
[30] K. Edalati, T. Fujioka, Z. Horita, Mater. Sci. Eng. A 497 (2008) 168–173.
[31] H.P. Stuwe, Acta Metall. 13 (1965) 1337–1342.
[32] M. Zehetbauer, Acta Metall. Mater. 41 (1993) 589–599.
[33] N. Hansen, Metall. Mater. Trans. A 32 (2001) 2917–2935.
[34] ISO 5832-2, Implants for Surgery –Metallic Materials – Part 2: Unalloyed Titanium, International Standardization Organization, Geneva, 1990.
[35] M. Tkacz, R. Burtovyy, Solid State Commun. 132 (2004) 37–41.
[36] M. Tkacz, R. Burtovyy, J. Alloys Compd. 404–406 (2005) 368–371.
[37] C.Q. Cheny, S.X. Li, K. Lu, Philos. Mag. 84 (2004) 29–43.
[38] D.S. Shih, I.M. Robertson, H.K. Birnbaum, Acta Metall. 36 (1988) 111–124.
[39] S. Gahr, M.L. Grossbeck, H.K. Birnbaum, Acta Metall. 25 (1977) 125–134.
[40] H.K. Birnbaum, M.L. Grossbeck, M. Amano, J. Less-Common Met. 49 (1976) 357–370.
[41] S. Takano, T. Suzuki, Acta Metall. 22 (1974) 265–274.
[42] R.A. Oriani, Acta Metall. 18 (1970) 147–157.
[43] T.B. Flannagan, N.B. Mason, H.K. Birnbaum, Scr. Metall. 15 (1981) 109–112.
[44] M.P. Puls, Acta Metall. 32 (1984) 1259–1269.
[45] J. Lufrano, P. Sofronis, H.K. Birnbaum, J. Mech. Phys. Solids 44 (1996) 179–205.
[46] T. Ogawa, K. Yokoyama, K. Asaoka, J. Sakai, J. Alloys Compd. 396 (2005) 269–274.